A Comparison of Numerical Flux Formulas for the Euler Equations
- Math 671 final assignment -

H. Nishikawa*

December 1998

Abstract

In this report, eight basic numerical flux functions for 1D Euler equations are compared on Sod's shock tube problems. Some fundamental properties of the schemes will be discussed. Also a solution obtained by a second-order method will be presented.

1 Introduction

In this study, we consider the 1D Euler equations for a perfect gas.

$$\frac{\partial \mathbf{u}}{\partial t} + \frac{\partial \mathbf{f}}{\partial x} = 0 \tag{1}$$

where

$$\mathbf{u} = [\rho, \rho u, \rho E]^T, \quad \mathbf{f} = \left[\rho u, \rho u^2 + p, \rho u H\right]^T, \quad \rho E = \rho H - p = \frac{p}{\gamma - 1} + \frac{1}{2}\rho u^2, \quad \gamma = 1.4. \tag{2}$$

We write a numerical scheme in the conservative form.

$$\mathbf{U}_j^{n+1} = \mathbf{U}_j^n - \frac{\Delta t}{\Delta x}\left(\mathbf{F}_{j+\frac{1}{2}} - \mathbf{F}_{j-\frac{1}{2}}\right) \tag{3}$$

where $\mathbf{U}_j^n$ is a numerical approximation to the cell-average of the exact solution over the j^{th} cell at $t = t_n$, and $\mathbf{F}_{j+\frac{1}{2}}$ is a numerical flux approximating the time-average of the exact flux over Δt evaluated at $x_{j+\frac{1}{2}}$.

Various formulas for the numerical flux have been developed up to the present. We shall consider eight of those in this report. Although these schemes are derived from different interpretations of the numerical approximation; computing cell-averages(finite-volume method) or point-values(finite difference method), it is not an important issue here since we consider only 1st/2nd order method.

2 Numerical Fluxes

In this section, we will give the formulas for the numerical flux, and describe some well-known properties for each.

*Doctoral Candidate, Aerospace Engineering and Scientific Computing

2.1 Lax-Friedrichs scheme

Lax-Friedrichs' scheme, written in the conservation form, is defined by the following flux function.

$$\mathbf{F}_{j+\frac{1}{2}} = \frac{1}{2}\left[f(\mathbf{U}_j^n) + f(\mathbf{U}_{j+1}^n)\right] - \frac{\Delta x}{2\Delta t}\left[\mathbf{U}_{j+1}^n - \mathbf{U}_j^n\right]. \tag{4}$$

It is well-known that the scheme is very dissipative. In the linear case, it can be shown that the amplitude error gets larger as the CFL number goes down.

2.2 Richtmyer's scheme

Richtmyer's scheme is a two-step Lax-Wendroff type scheme defined by

$$\mathbf{U}_{j+\frac{1}{2}}^{n+\frac{1}{2}} = \frac{1}{2}\left[\mathbf{U}_j^n + \mathbf{U}_{j+1}^n\right] - \frac{\Delta t}{2\Delta x}\left[f(\mathbf{U}_{j+1}^n) - f(\mathbf{U}_j^n)\right] \tag{5}$$

$$\mathbf{U}_j^{n+1} = \mathbf{U}_j^n - \frac{\Delta t}{\Delta x}\left[f(\mathbf{U}_{j+\frac{1}{2}}^{n+\frac{1}{2}}) - f(\mathbf{U}_{j-\frac{1}{2}}^{n+\frac{1}{2}})\right]. \tag{6}$$

This is in the conservative form, and therefore we identify Richtmyer's flux function as

$$\mathbf{F}_{j+\frac{1}{2}} = f(\mathbf{U}_{j+\frac{1}{2}}^{n+\frac{1}{2}}) \tag{7}$$

with (5).

The first step is the Lax-Friedrichs scheme, and the second is a leapfrog scheme. This scheme becomes identical to the Lax-wendroff scheme in the linear case. The Lax-wendroff scheme is known as dispersive, i.e. high frequency components lag behind. And due to the small dissipation they remain to be high frequency. A linear analysis tells us that this behavior becomes more conspicuous as the CFL number goes down.

2.3 MacCormack's scheme

MacCormack's scheme is also a two-step Lax-Wendroff type scheme defined by

$$\mathbf{U}_j^* = \mathbf{U}_j^n - \frac{\Delta t}{\Delta x}\left[f(\mathbf{U}_{j+1}^n) - f(\mathbf{U}_j^n)\right] \tag{8}$$

$$\mathbf{U}_j^{n+1} = \frac{1}{2}\left[\mathbf{U}_j^n + \mathbf{U}_j^*\right] - \frac{\Delta t}{2\Delta x}\left[f(\mathbf{U}_j^*) - f(\mathbf{U}_{j-1}^*)\right]. \tag{9}$$

MacCormack's scheme is known as conservative. Indeed it can be written in the conservative form by substituting (8) into (9) and defining the numerical flux as

$$\mathbf{F}_{j+\frac{1}{2}} = \frac{1}{2}\left[f(\mathbf{U}_{j+1}^n) + f(\mathbf{U}_j^*)\right] \tag{10}$$

with (8).

This also becomes identical to the Lax-wendroff scheme in the linear case. The first step is a first order forward difference, and the second is a backward difference. Therefore, either step will be unstable for one characteristic speed, but the overall scheme is stable and of second-order in the linear case. In nonlinear cases however, it is well-known to suffer a nonlinear instability due to the lack of dissipation. Another important property of the scheme is that it fails at the sonic expansion, as Roe's method does, due to the upwind nature.

2.4 Steger-Warming scheme (the beam scheme)

We apply the upwind scheme for a positive and a negative part of the flux separately.

$$\mathbf{F}_{j+\frac{1}{2}} = \mathbf{f}^+(\mathbf{U}_j^n) + \mathbf{f}^-(\mathbf{U}_{j+1}^n). \tag{11}$$

In Steger-Warming splitting, we project the flux onto the space of eigenvectors using the homogeneity property, and split the flux. This results

$$\mathbf{f}^{\pm}(\mathbf{U}) = \lambda^{(1)\pm}\frac{\rho}{2\gamma}\begin{bmatrix}1\\ u-c\\ H-uc\end{bmatrix} + \lambda^{(2)\pm}\frac{\rho\,(\gamma-1)}{\gamma}\begin{bmatrix}1\\ u\\ \frac{1}{2}u^2\end{bmatrix} + \lambda^{(3)\pm}\frac{\rho}{2\gamma}\begin{bmatrix}1\\ u+c\\ H+uc\end{bmatrix} \tag{12}$$

where

$$\lambda^{(k)\pm} = \frac{\lambda^{(k)} \pm |\lambda^{(k)}|}{2}, \quad k = 1, 2, 3. \tag{13}$$

and $\lambda^{(k)}$ are defined by

$$\lambda^{(1)} = u - c,\ \lambda^{(2)} = u,\ \lambda^{(3)} = u + c. \tag{14}$$

The vectors are, as mentioned, associated eigenvectors, $r^{(1)}$, $r^{(2)}$, and $r^{(3)}$ respectively. This is however not a unique splitting of the flux. It is a disadvantage of this splitting that it is not differentiable at a sonic and stagnation points. Later Van Leer designed a splitting that is differentiable.

2.5 Van Leer's scheme

Applying upwind differencing, we again write the numerical flux as

$$\mathbf{F}_{j+\frac{1}{2}} = \mathbf{f}^+(\mathbf{U}_j^n) + \mathbf{f}^-(\mathbf{U}_{j+1}^n) \tag{15}$$

where Van Leer's flux vector splitting reads

$$\mathbf{f}^+(\mathbf{U}) = \frac{\rho c}{4}(M+1)^2\begin{bmatrix}1\\ \frac{2c}{\gamma}\left(1+\frac{\gamma-1}{2}M\right)\\ \frac{2c^2}{\gamma^2-1}\left(1+\frac{\gamma-1}{2}M\right)^2\end{bmatrix},\quad \mathbf{f}^-(\mathbf{U}) = -\frac{\rho c}{4}(M-1)^2\begin{bmatrix}1\\ \frac{2c}{\gamma}\left(-1+\frac{\gamma-1}{2}M\right)\\ \frac{2c^2}{\gamma^2-1}\left(1-\frac{\gamma-1}{2}M\right)^2\end{bmatrix} \tag{16}$$

where M is the Mach number. This is differentiable at a sonic and a stagnation points.

2.6 Godunov's scheme

Godunov's scheme is the one that solves the Riemann problem at each interface exactly. The details of the algorithm can be found in [1]. Note that this is a first-order method because of the assumption of piecewise constant data.

2.7 Osher's scheme

Osher's scheme is an approximate Riemann solver. The derivation is so involed (the detailed derivation is attached) that it will not be described here. It is written as

$$\mathbf{F}_{j+\frac{1}{2}} = \frac{1}{2}\left[\mathbf{f}(\mathbf{U}_j^n) + \mathbf{f}(\mathbf{U}_{j+1}^n)\right] - \frac{1}{2}\int_j^{j+1} |\mathbf{A}(\mathbf{U})|\, d\mathbf{U} \tag{17}$$

where $\mathbf{A}$ is the Jacobian matrix $\frac{\partial \mathbf{f}}{\partial \mathbf{u}}$. The integral is to be broken into three parts,

$$\int_j^{j+1} |\mathbf{A}(\mathbf{U})|\, d\mathbf{U} = \int_j^{Lm} |\mathbf{A}(\mathbf{U})|\, d\mathbf{U} + \int_{Lm}^{Rm} |\mathbf{A}(\mathbf{U})|\, d\mathbf{U} + \int_{Rm}^{j+1} |\mathbf{A}(\mathbf{U})|\, d\mathbf{U} \tag{18}$$

where the integrals are carried out along right eigenvectors, $r^{(3)}$, $r^{(2)}$, and $r^{(1)}$ respectively. After some analysis, we arrive at the following practical(ready-to-use) formula.

$$\mathbf{F}_{j+\frac{1}{2}} = \frac{1}{2}\left[\mathbf{f}(\mathbf{U}_j^n) + \mathbf{f}(\mathbf{U}_{j+1}^n)\right] - \frac{1}{2}\left[\mathbf{F} + \mathbf{F}_{3\text{-sonic}} + \mathbf{F}_{1\text{-sonic}}\right] \tag{19}$$

where

$$\begin{aligned}
\mathbf{F} &= \mathrm{sgn}(\lambda_j^{(3)})\ \mathbf{f}(\mathbf{U}_j) + \mathrm{sgn}(\lambda_{j+1}^{(1)})\ \mathbf{f}(\mathbf{U}_{j+1}) && (20)\\
&\quad + \left[\mathrm{sgn}(\lambda_j^{(3)}) - \mathrm{sgn}(\lambda_{Lm}^{(2)})\right]\ \mathbf{f}(\mathbf{U}_{Lm}) && (21)\\
&\quad + \left[\mathrm{sgn}(\lambda_{Lm}^{(2)}) - \mathrm{sgn}(\lambda_{j+1}^{(1)})\right]\ \mathbf{f}(\mathbf{U}_{Rm}) && (22)
\end{aligned}$$

and

$$\mathbf{F}_{3\text{-sonic}} = \begin{cases} 2\mathrm{sgn}(\lambda_j^{(3)})\left[\mathbf{f}(\mathbf{U}^*) - \mathbf{f}(\mathbf{U}_{Lm})\right] & \lambda_j^{(3)} \cdot \lambda_{Lm}^{(3)} < 0 \\ 0 & \text{otherwise} \end{cases} \tag{23}$$

$$\mathbf{F}_{1\text{-sonic}} = \begin{cases} 2\mathrm{sgn}(\lambda_{j+1}^{(1)})\left[\mathbf{f}(\mathbf{U}_{Rm}) - \mathbf{f}(\mathbf{U}^*)\right] & \lambda_{j+1}^{(1)} \cdot \lambda_{Rm}^{(1)} < 0 \\ 0 & \text{otherwise} \end{cases} \tag{24}$$

The intermediate states, Lm and Rm, can be found easily. And $\mathbf{U}^*$ is the state of the sonic point at which $\lambda^{(k)} = 0, k = 1$ or 3, which can also be determined easily.

Clearly, the approximate Riemann solution does not contain discontinuous transition(integrations along $r^{(k)}$, not the Hugoniot curve.). According to Van Leer's analysis, the integration can be interpreted as along an overturned shock in phase space whenever there exists a discontinuity in reality. The resulting solution however will be sharp with at most two interior cells.

2.8 Roe's scheme

Roe's scheme is an approximate Riemann solver based on a linearization. The scheme reads

$$\mathbf{F}_{j+\frac{1}{2}} = \frac{1}{2}\left[\mathbf{f}(\mathbf{U}_j^n) + \mathbf{f}(\mathbf{U}_{j+1}^n)\right] - \frac{1}{2}\sum_{k=1}^{3} |\hat{\lambda}^{(k)}| \Delta\hat{V}^{(k)} \hat{r}^{(k)} \tag{25}$$

where $\Delta V^{(k)}$ is the discretized kth component of the differential of the characteristic vector,

$$\Delta\hat{V}^{(k)} = \left[\frac{\Delta p - \hat{\rho}\hat{c}\Delta u}{2\hat{c}^2},\ -\frac{\Delta p - \hat{c}^2\Delta\rho}{\hat{c}^2},\ \frac{\Delta p + \hat{\rho}\hat{c}\Delta u}{2\hat{c}^2}\right] \tag{26}$$

where $\Delta p = p_R - p_L = p_{j+1} - p_j$, and similarly for others. And $\hat{r}^{(k)}$ are right eigenvectors

$$\hat{r}^{(1)} = \left[1,\ \hat{u} - \hat{c},\ \hat{H} - \hat{u}\hat{c}\right]^T,\ \hat{r}^{(2)} = \left[1,\ \hat{u},\ \frac{\hat{u}^2}{2}\right]^T,\ \hat{r}^{(3)} = \left[1,\ \hat{u} + \hat{c},\ \hat{H} + \hat{u}\hat{c}\right]^T. \tag{27}$$

with the eigenvalues

$$\hat{\lambda}^{(1)} = \hat{u} - \hat{c},\ \hat{\lambda}^{(2)} = \hat{u},\ \hat{\lambda}^{(3)} = \hat{u} + \hat{c}. \tag{28}$$

All the quantities with a hat are evaluated by the Roe-averages,

$$\hat{\rho} = \sqrt{\rho_L\rho_R} = R\,\rho_L,\ \ \hat{u} = \frac{u_L + R\,u_R}{1+R},\ \ \hat{H} = \frac{H_L + R\,H_R}{1+R},\ \ \hat{c}^2 = (\gamma-1)\left(\hat{H} - \frac{\hat{u}^2}{2}\right). \tag{29}$$

In Roe's method, all the waves are replaced by linear waves, and therefore no rarefaction waves(nonlinear waves) are contained in the scheme. This results in the failure of detecting the sonic point, and it needs to be modified in such a case.

3 Results and Discussions

We consider the following shock tube problem(no sonic rarefaction).

$$\begin{cases} \rho_L = 1.0,\ p_L = 1.0,\ u_L = 0.0 & x \le 0 \\ \rho_R = 0.125,\ p_R = 0.1,\ u_R = 0.0 & x > 0 \end{cases} \tag{30}$$

We define the CFL number by

$$\text{CFL} = \frac{\max_{cells}(|u_j| + c_j)\Delta t}{\Delta x}. \tag{31}$$

We will use a uniform grid with 80 cells, and use the CFL number as a parameter (0 <CFL$\le$ 1). Therefore Δt will be computed, from the above relation, at each time step to keep the CFL number as specified. And we will stop the calculation when time exceeds 1.7. As a boundary condition, we place two ghost cells at each end and store the same solutions as the adjacent cells'. We computed the solutions for two CFL numbers, CFL=0.95 and 0.1, to see how the properties of the schemes in the linear case are carried over to the nonlinear case. Finally the solid lines in all the figures that follow indicate the exact solutions.

Lax-Friedrichs (Figures 1 and 2)

We see clearly the effect of its large dissipation. And as we expected from the linear analysis, it gets worse as we reduce the CFL number. Also the staircase-like solution, which is particular to the Lax-Friedrichs scheme, is observed.

Two-step LW-type schemes(Richtmyer, MacCormack) (Figures 3-6)

In both cases, the solution is oscillatory due to the dispersive property of second-order schemes although the solutions are more accurate than those obtained by first-order methods in the smooth regions. As we expected, the oscillations grow (in fact *remain* due to the lack of dissipation) as the CFL number goes down. In particular, MacCormack's scheme breaks down for CFL < 0.6518. This is often called nonlinear instability since the scheme is theoretically stable for CFL ≤ 1 in the linear case. On the other hand, Richtmyer does not break down due to the large dissipation introduced in its first step(Lax-Friedrichs), but still exhibits a highly oscillatory behavior. It is nevertheless well-known that the oscillations can be surpressed by introducing some artificial viscosity at the cost of the introduction of a problem-dependent tuning parameter[1].

Upwind schemes(Steger-Warming, Van Leer, Godunov, Osher, Roe) (Figures 7-16)

In the linear case, we know the upwind scheme works quite well, i.e. less dissipative than Lax-Friedrichs' scheme, and low dispersion error. It is clearly seen from the results that these properties remain in the nonlinear case.

From the above observations, we see that the properties of the schemes well-known in the linear case are indeed carried over to the nonlinear case. We then could conclude that we obtain the best results by the upwind schemes. Next we compare the upwind schemes.

Steger-Warming, Van Leer, Godunov, Osher, Roe (Figures 7, 9, 11, 13, and 15)

As can be seen in figure 7 and 9, Van Leer's scheme improves the solution at the contact discontinuity and at both ends of the expansion fan, compared with those by Steger-Warming's scheme in which the solution is strongly smeared out at these regions. For Godunov-type methods, Godunov, Osher, and Roe, the solutions are almost indistinguishable. This leads us to conclude that Roe's method be the practical choice since it requires the least computational work among the three. Now, we compare Van Leer and Roe, Figures 7 and 15. There is no significant differences except for a minor difference in the expansion fan. It is hard to tell at this point which is superior in a general sense. Finally note that the contact discontinuity is smeared significantly in all the schemes, which can be seen clearly in the entropy plot. On the other hand, the shock has been resolved quite sharply by most of the schemes. This is

a typical result for a nonlinear discontinuity because of its self-sharpening nature (combination of the characteristics merging into the shock and the upwind method) while there is no such mechanism in the linearly degenerate field (combination of the characteristics running parallel to the discontinuity and the upwind method, i.e. upwind in the same direction across the discontinuity).

In the sense of extending the first-order method to the second-order, it would be reasonable to choose Roe's method because of its linearization property. A second-order method developed for a linear system can be applied directly to the Euler equations linearized by the method of Roe.

MUSCL scheme with Roe-linearization (Figures 17)

There are various ways to extend the first- order method to the second-order accuracy. In this study, the method described in [2] was used. We first construct a set of piecewise linear data within each cell with the minmod limiter, then solve the linearized characteristic equations (linear advection) exactly, and finally average the solutions. All these steps being put together, the flux can be written, on a uniform grid,

$$\mathbf{F}_{j+\frac{1}{2}} = \mathbf{F}_{\text{upwind}} + \frac{1}{2}\sum_{p=1}^{3} \hat{\lambda}^{(p)} \left(\text{sgn}(\hat{\nu}^{(p)}) - \hat{\nu}^{(p)}\right) \sigma_{i_p}^{(p)} \hat{r}^{(p)} \tag{32}$$

where $\mathbf{F}_{\text{upwind}}$ is the upwind flux given by (25), $\hat{\nu}^{(p)} = \hat{\lambda}^{(p)} dt/dx$, and

$$\sigma_j^{(p)} = \text{minmod}(d\hat{V}_{j+\frac{1}{2}}^{(p)}, d\hat{V}_{j-\frac{1}{2}}^{(p)}) \tag{33}$$

$$i_p = \begin{cases} j & \text{if} \quad \hat{\lambda}^{(p)} > 0 \\ j+1 & \text{if} \quad \hat{\lambda}^{(p)} < 0 \end{cases} \tag{34}$$

Note that all the quantities with a hat are evaluated by the Roe-averages between jth and $(j+1)$th cells except for $d\hat{V}_{j-\frac{1}{2}}^{(p)}$ and $d\hat{V}_{j+\frac{3}{2}}^{(p)}$ which must be evaluated by the Roe-averages between their corresponding two neighboring cells.

As shown in figures 17 and 18, a noticeable improvement can be seen especially at the contact discontinuity. The oscillations typical to second-order schemes have been successfully removed by the minmod limiter.

Sonic rarefaction (Figures 19-24)

Finally, we compare some of the schemes for the case of sonic rarefaction. The initial values are taken from [3],

$$\begin{cases} \rho_L = 3.857,\ p_L = 10.333,\ u_L = 0.92 & x \le 0 \\ \rho_R = 1.0,\ p_R = 1.0,\ u_R = 3.55 & x > 0 \end{cases} \tag{35}$$

First of all, MacCormack's and Roe's schemes keep the nonphysical discontinuity as expected. Also Van Leer's scheme breaks down for any value of the CFL number. As shown in Figure 19., Lax-Friedrichs works, but not quite well. It is too dissipative and also creates a large peak of entropy behind the contact discontinuity. Richtmyer(Figure 20) gives a good solution except the oscillation in the entropy behind the contact discontinuity. On the other hand, Steger-Warming scheme produces completely wrong solutions as can be seen in Figure 21. As in the previous test problem, Godunov and Osher give almost identical solutions. And they have a glitch at the soonic point as usually observed, and also create an entropy peak behind the contact discontinuity although small compared with others. Finally, Roe's method was applied with an entropy fix, modifying the wave speed by a smooth quadratic function near the sonic point as described in [1]. It is clearly seen in Figure 24 that the solution is much smoother at the sonic point than other schemes. However, it creates a quite large entropy peak behind the contact discontinuity.

4 Concluding Remarks

The eight basic schemes for the Euler equations were compared for two shock tube problems. From this study, the following conclusions may be drawn. First, the upwind schemes would be the best choice for the Euler equations. Second, the flux-vector splitting methods are not as robust as Godunov-type methods as shown in the case of the sonic rarefaction. But Godunov-type methods can produce a spurious solution in some cases.

References

[1] Hirsch, C., *Numerical Computation of Internal and External Flows*, Volume 2, John Wiley & Sons, 1990.

[2] LeVeque, R. J., *Numerical Methods for Conservation Laws*, Birkhäuser, 1992.

[3] Huynh, H. T., Accurate Upwind Methods for the Euler Equations, *SIAM J. Num. Anal.*, Vol. **32**, No. 5, pp. 1565-1619, October 1995.

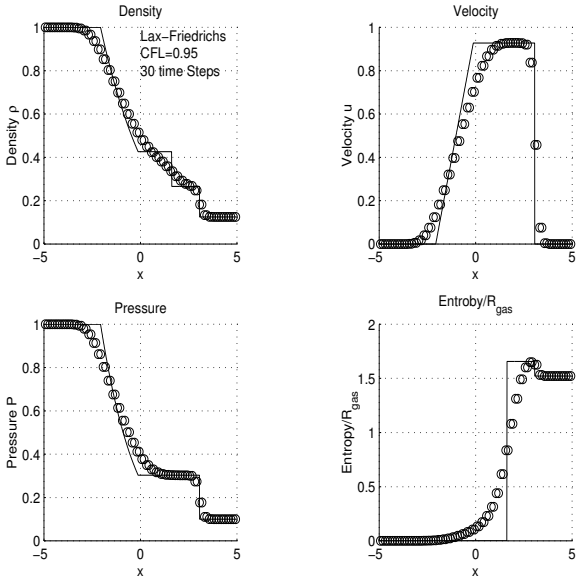

Figure 1: The solutions by Lax-Friedrichs' scheme with CFL= 0.95, $t = 1.74833$.

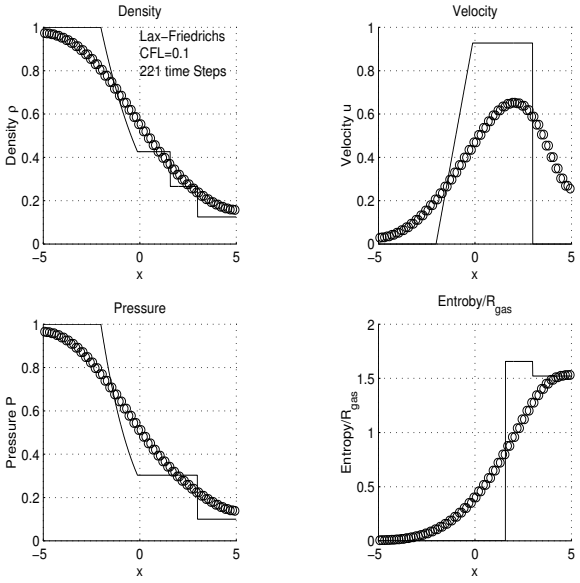

Figure 2: The solutions by Lax-Friedrichs' scheme with CFL= 0.1, $t = 1.70464$.

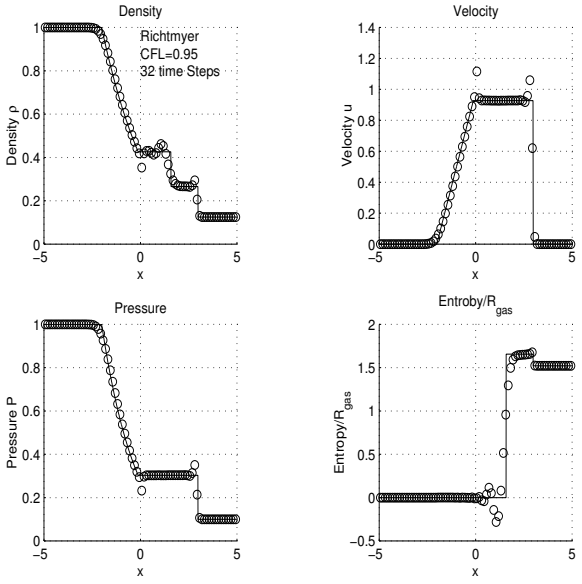

Figure 3: The solutions by Richtmyer's scheme with CFL= 0.95, $t = 1.70154$.

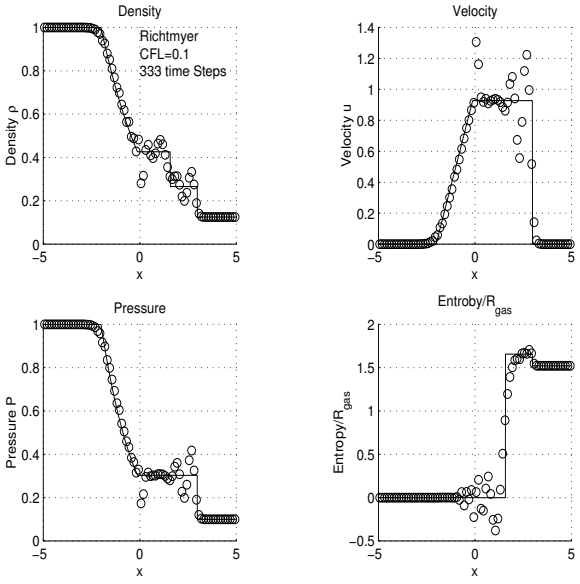

Figure 4: The solutions by Richtmyer's scheme with CFL= 0.1, $t = 1.70036$.

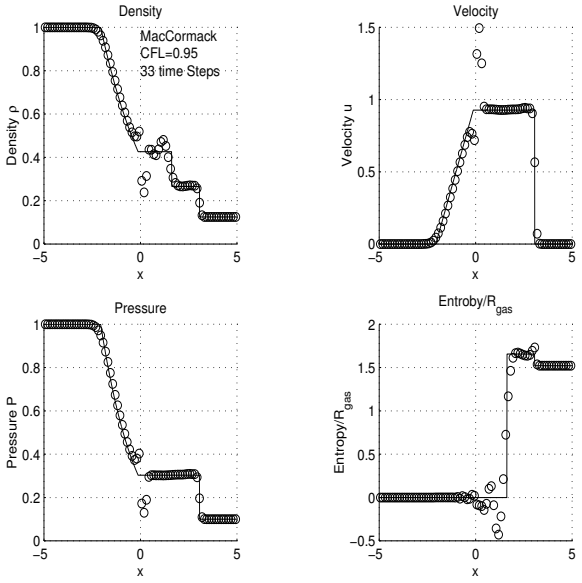

Figure 5: The solutions by MacCormack's scheme with CFL= 0.95, $t = 1.74408$.

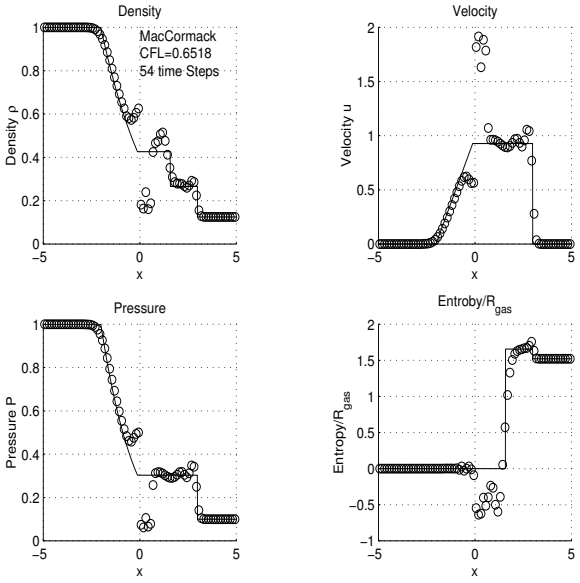

Figure 6: The solutions by MacCormack's scheme with CFL= 0.6518, $t = 1.73141$.

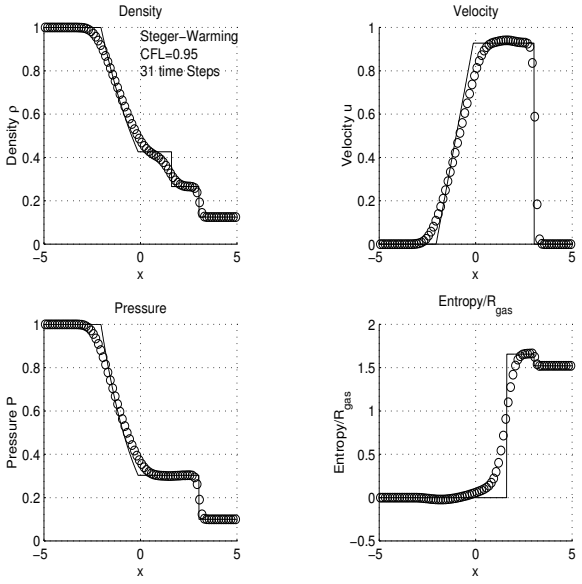

Figure 7: The solutions by Steger-Warming scheme with CFL= 0.95, $t = 1.73133$.

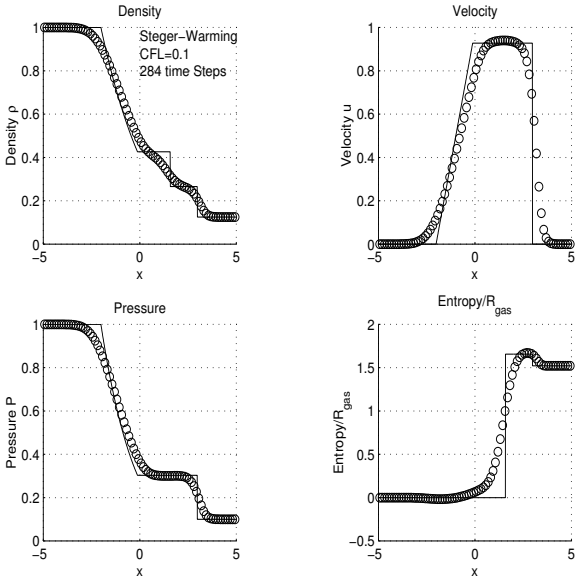

Figure 8: The solutions by Steger-Warming scheme with CFL= 0.1, $t = 1.70308$.

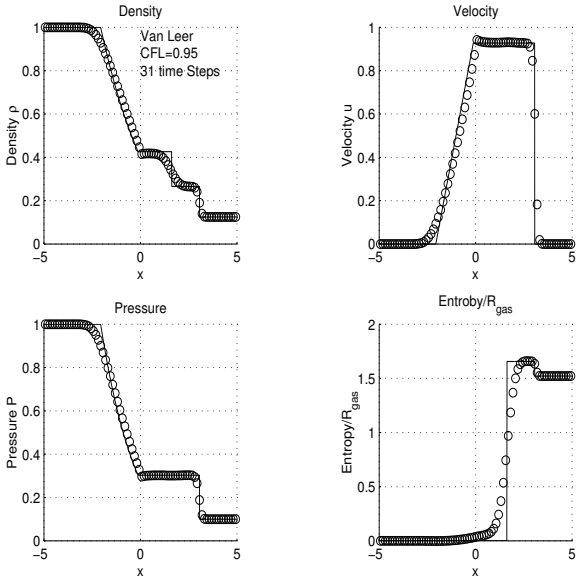

Figure 9: The solutions by Van Leer's scheme with CFL= 0.95, $t = 1.74534$.

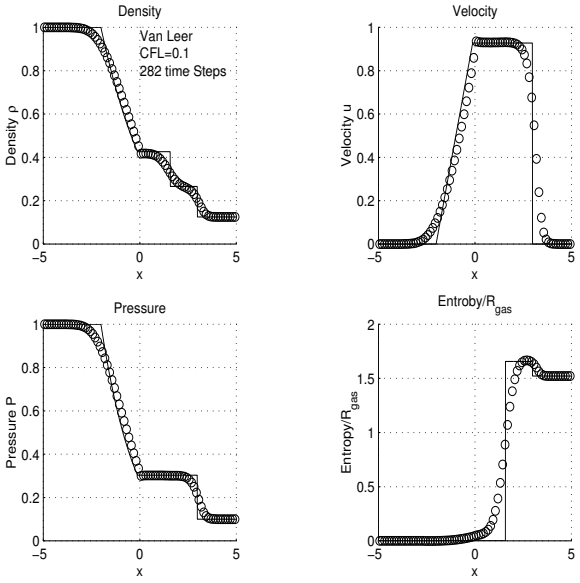

Figure 10: The solutions by Van Leer's scheme with CFL= 0.1, $t = 1.70217$.

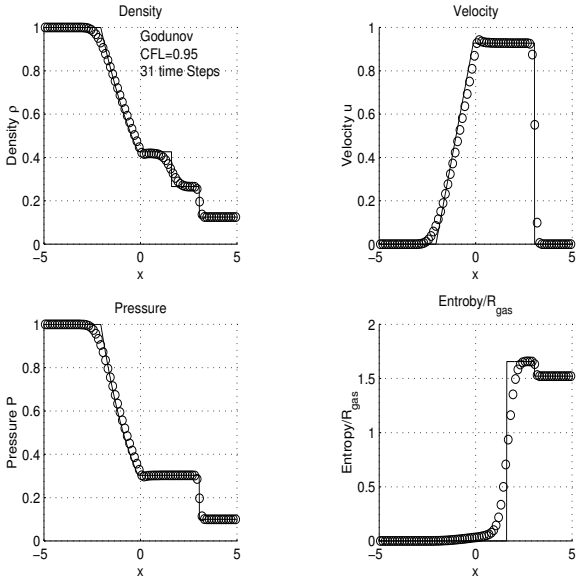

Figure 11: The solutions by Godunov's scheme with CFL= 0.95, $t = 1.73846$.

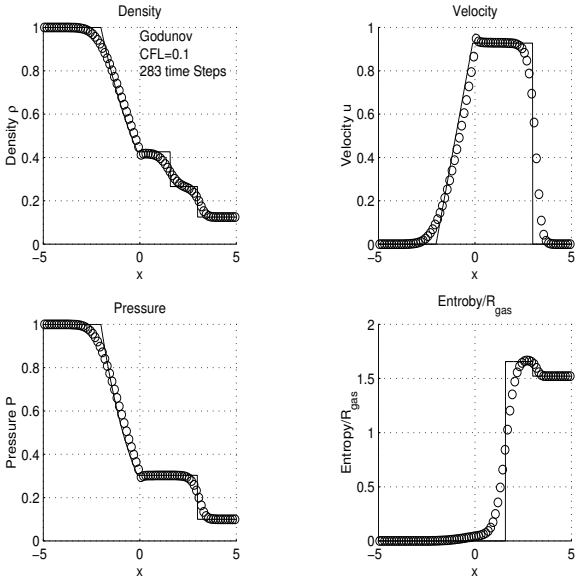

Figure 12: The solutions by Godunov's scheme with CFL= 0.1, $t = 1.70409$.

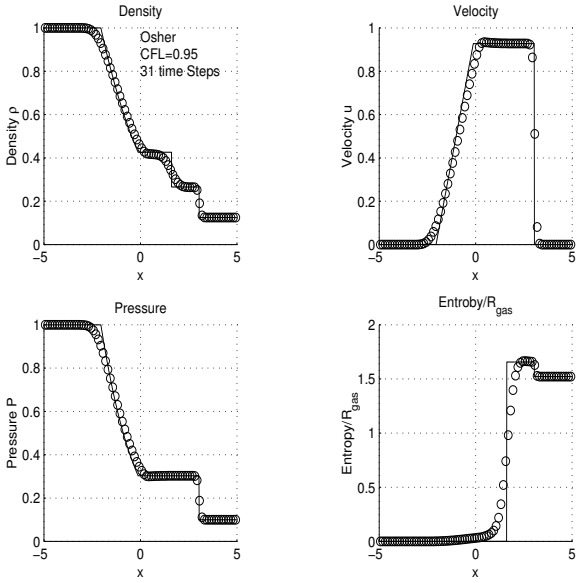

Figure 13: The solutions by Osher's scheme with CFL= 0.95 at $t = 1.73402$.

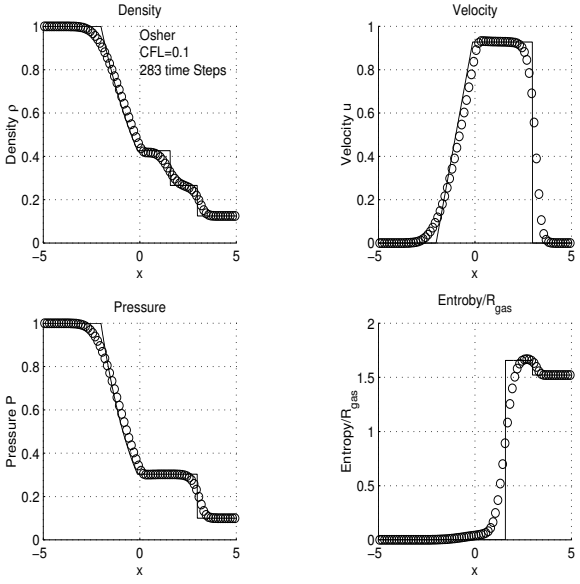

Figure 14: The solutions by Osher's scheme with CFL= 0.1, $t = 1.70201$.

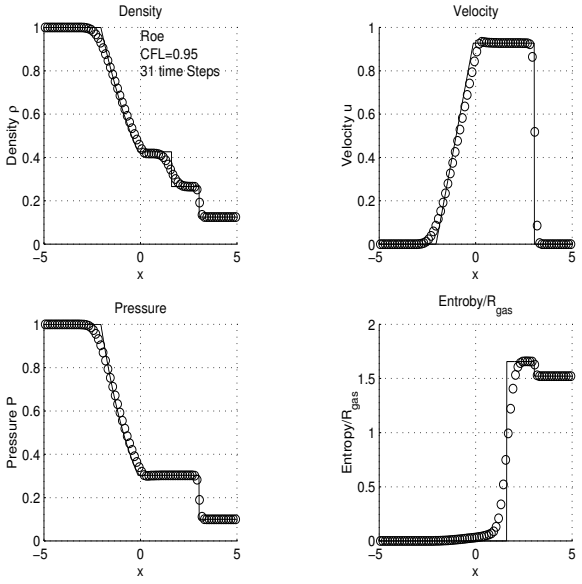

Figure 15: The solutions Roe's scheme with CFL= 0.95, $t = 1.73448$.

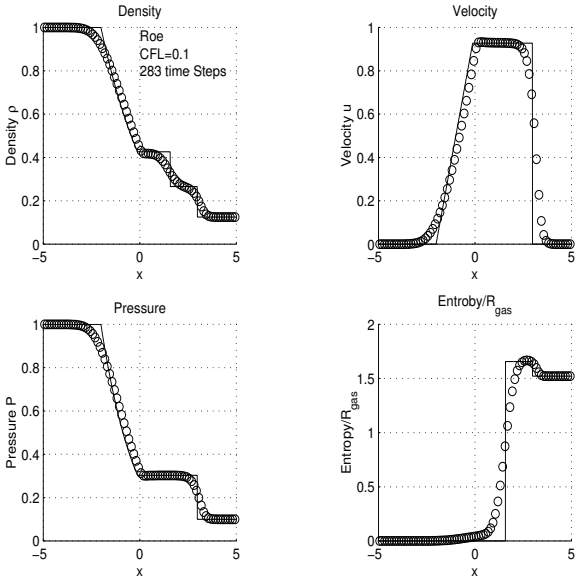

Figure 16: The solutions by Roe's scheme with CFL= 0.1, $t = 1.70268$.

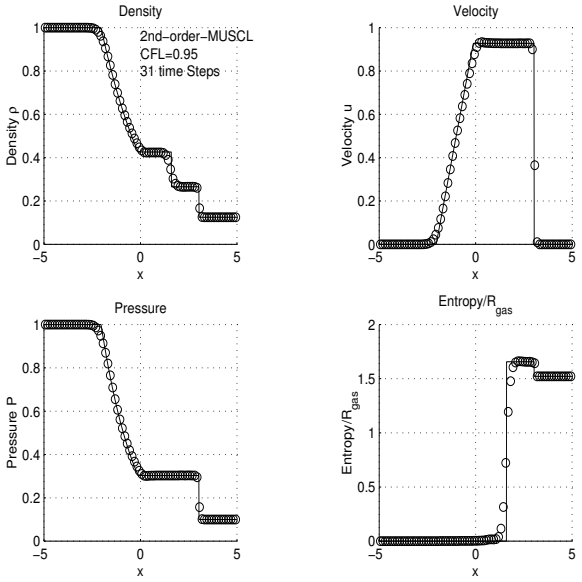

Figure 17: Second-order solution by MUSCL with CFL= 0.95, $t = 1.72672$.

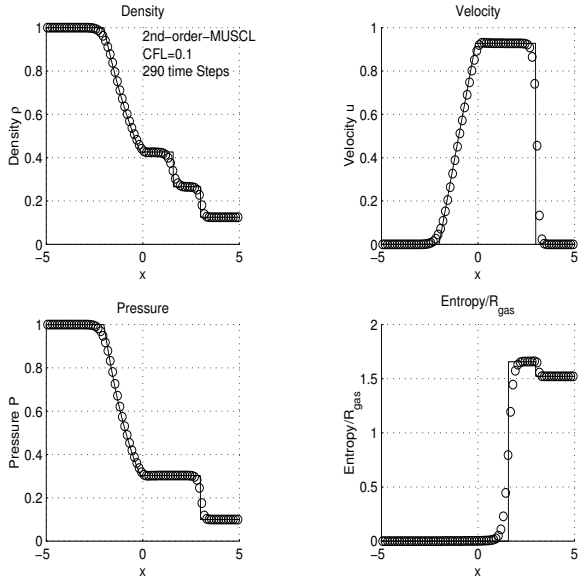

Figure 18: Second-order solution by MUSCL with CFL= 0.1, $t = 1.70463$.

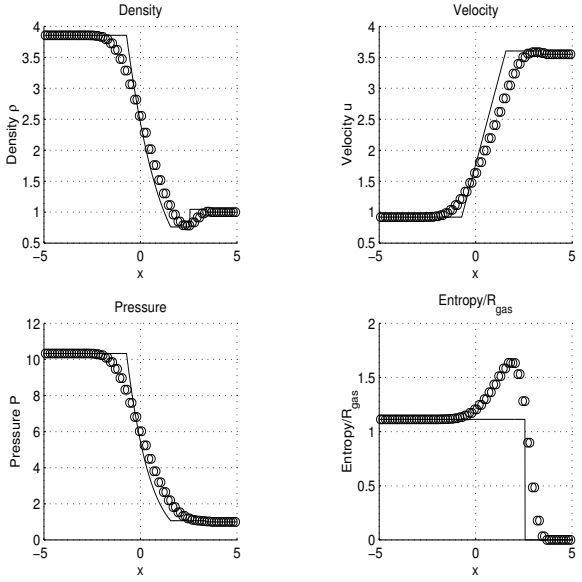

Figure 19: Lax-Friedrichs for the sonic rarefaction with CFL= 0.95, 29 time steps, $t = 0.711396$.

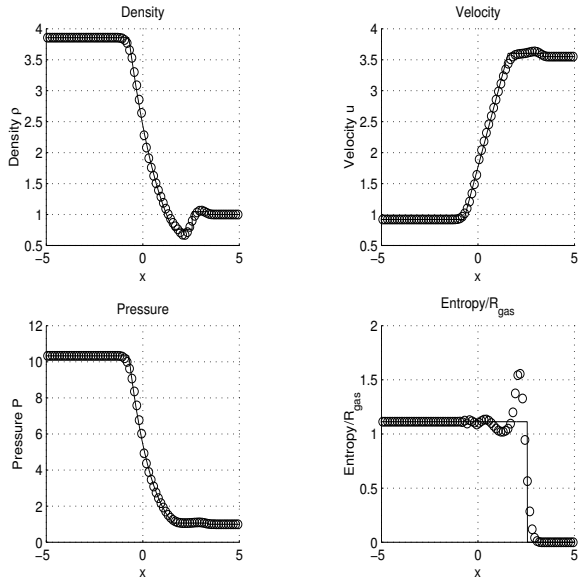

Figure 20: Richtmyer for the sonic rarefaction with CFL= 0.95, 30 time steps, $t = 0.711278$.

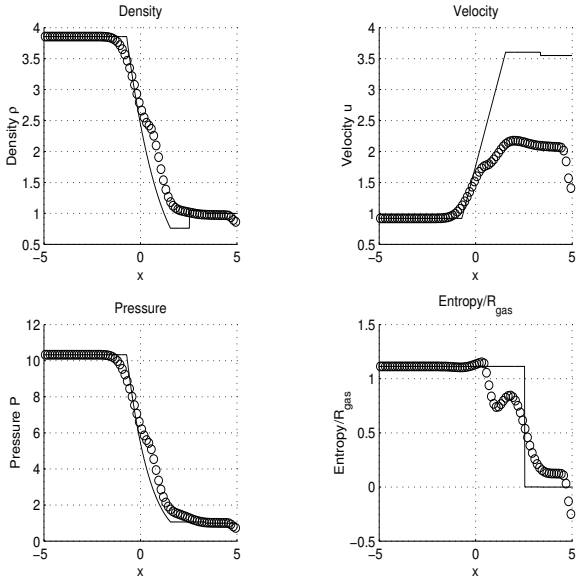

Figure 21: Steger-Warming for the sonic rarefaction CFL= 0.3, 77 time steps, $t = 0.705027$.

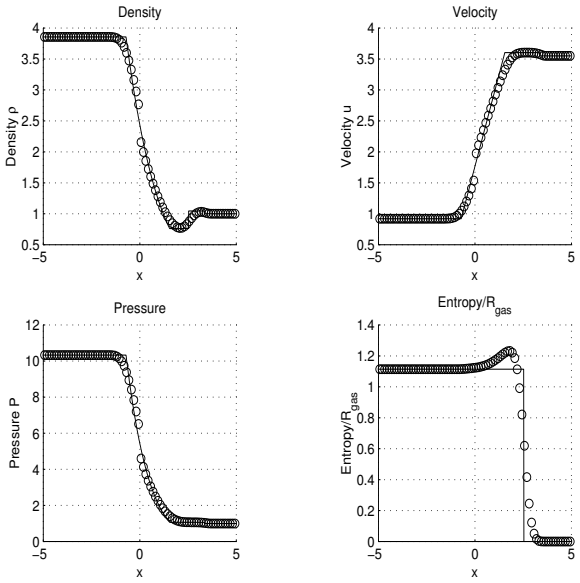

Figure 22: Godunov for the sonic rarefaction with CFL= 0.95, 29 time steps, $t = 0.70471$.

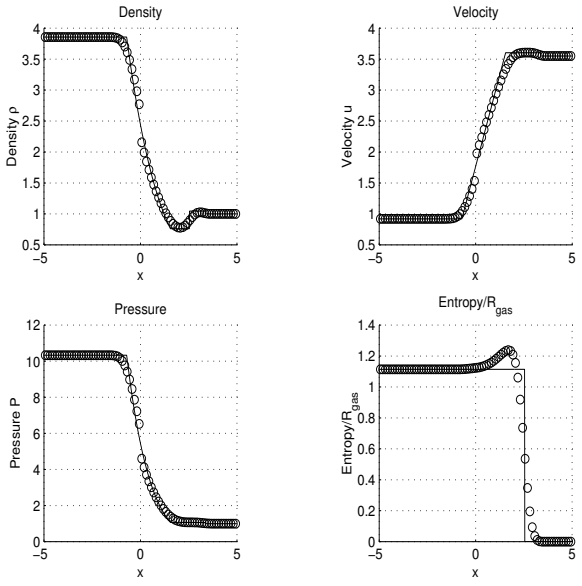

Figure 23: Osher for the sonic rarefaction with CFL= 0.95, 29 time steps, $t = 0.70471$.

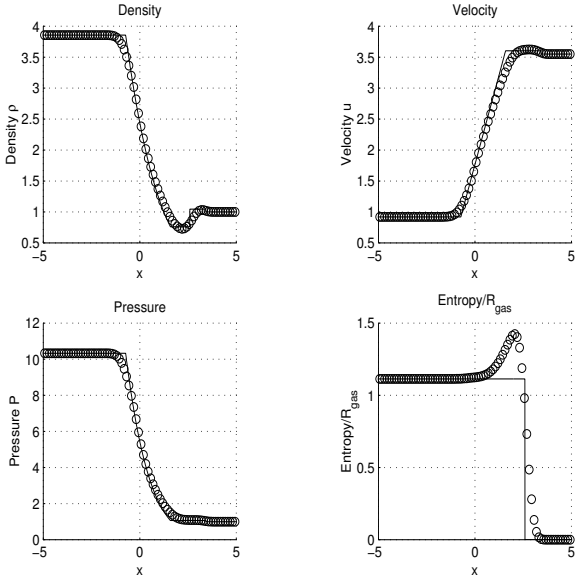

Figure 24: Roe's scheme with an entropy fix for the sonic rarefaction CFL= 0.95, 30 time steps, $t = 0.719955$.